Cellular Deformations Induced by Conical Silicon Nanowire Arrays Facilitate Gene Delivery

Yaping Chen, Stella Aslanoglou, Gediminas Gervinskas, Hazem Abdelmaksoud, Nicolas H. Voelcker,* and Roey Elnathan*

Engineered cell–nanostructured interfaces generated by vertically aligned silicon nanowire (SiNW) arrays have become a promising platform for orchestrating cell behavior, function, and fate. However, the underlying mechanism in SiNW-mediated intracellular access and delivery is still poorly understood. This study demonstrates the development of a gene delivery platform based on conical SiNW arrays for mechanical cell transfection, assisted by centrifugal force, for both adherent and nonadherent cells in vitro. Cells form focal adhesions on SiNWs within 6 h, and maintain high viability and motility. Such a functional and dynamic cell–SiNW interface features conformational changes in the plasma membrane and in some cases the nucleus, promoting both direct penetration and endocytosis; this synergistically facilitates SiNW-mediated delivery of nucleic acids into immortalized cell lines, and into difficult-to-transfect primary immune T cells without pre-activation. Moreover, transfected cells retrieved from SiNWs retain the capacity to proliferate—crucial to future biomedical applications. The results indicate that SiNW-mediated intracellular delivery holds great promise for developing increasingly sophisticated investigative and therapeutic tools.

1. Introduction

Effective intracellular delivery of bioactive molecules into live cells is a powerful molecular tool for facilitating a plethora of progressive therapeutics, biosensing, and other biomedical applications.[1] Broadly, exogenous biomolecules can be delivered into cells via carrier-mediated transportation or cell membrane disruption.[2] For instance, viral vectors are one major type of carrier used for nucleic acid transfection.[3] Despite their high transfection efficiency,

notable weaknesses of viral vectors include expensive and time-consuming protocols, risk of immunogenicity, undesirable insertional genotoxicity, and restricted packaging capacity.[4] Nonviral carriers such as cationic lipids and polymers can condense nucleic acids into compact nanoparticles down to tens of nanometers,[5] which significantly enhances the efficiency of cargo delivery and confers protection against degradation by DNAases.[5a,6] But the potential disadvantages of complexation include delayed unpacking and lack of integration of exogenous DNA into the host genome, rendering gene expression inaccessible,[7] as well as excessive toxicity induced by the carriers.[8]

By contrast, membrane disruption-mediated methods are near-universal, capable of delivering almost any cargo into cells through direct penetration and/or indirect permeabilization.[2a] Multiple routes have been used to induce local membrane disruption, including mechanical (solid contact, fluid shear forces, and hydrostatic or osmotic pressure changes), electrical (electroporation), optical (optoporation), thermal, and chemical.[2b,c,9] Recently, diverse and tunable vertically configured nanostructures, including nanowire (NW) arrays,[10] nanotubes,[11] nanopillars,[12] nanoneedles,[13] nanocones,[14] and nanostraws,[15] have featured as mechanical platform, enabling powerful manipulation of cell functions and processes in vitro. McKnight et al. first produced vertically aligned carbon nanofibers that allowed

---

Dr. Y. Chen, S. Aslanoglou, Prof. N. H. Voelcker, Dr. R. Elnathan
Monash Institute of Pharmaceutical Sciences
Monash University
381 Royal Parade, Parkville, VIC 3052, Australia
E-mail: nicolas.voelcker@monash.edu; roey.elnathan@monash.edu

Dr. Y. Chen, S. Aslanoglou, H. Abdelmaksoud,
Prof. N. H. Voelcker, Dr. R. Elnathan
Melbourne Centre for Nanofabrication
Victorian Node of the Australian National Fabrication Facility
151 Wellington Road, Clayton, VIC 3168, Australia

Dr. Y. Chen, S. Aslanoglou, Prof. N. H. Voelcker
Commonwealth Scientific and Industrial Research Organisation (CSIRO)
Clayton, VIC 3168, Australia

Dr. G. Gervinskas
Ramaciotti Centre for Cryo-Electron Microscopy
Monash University
15 Innovation Walk, Clayton, VIC 3800, Australia

H. Abdelmaksoud
Future Industries Institute
University of South Australia
Mawson Lakes, SA 5095, Australia

Prof. N. H. Voelcker
INM-Leibniz Institute for New Materials
Campus D2 2, Saarbrücken 66123, Germany

**ADVANCED
SCIENCE NEWS**

www.advancedsciencenews.com

NANO · MICRO

small

www.small-journal.com

efficient DNA (green fluorescence protein (GFP) plasmid) transfection into live cells in 2004.[16] Other biomolecules—siRNA,[17] proteins,[17a,c,18] molecular beacons,[19] DNA nanocages,[20] impermeable drugs,[17a] and quantum dots,[21]—have since been delivered through NW arrays into a large variety of cell types, including difficult-to-transfect primary immune cells. A key study by Shalek et al. showed that an array of SiNWs can deliver siRNAs to silence *LEF1* expression in primary B cells without activating immune response, enabling study of the Wnt signaling pathway involved in chronic lymphocytic leukemia.[17b] Yosef et al. used NW arrays to inject siRNA into naïve mouse T helper 17 (Th17) and identified 39 (12 novel) regulatory genes for the differentiation of Th17 and other CD4+ T cell subsets.[22] Other NW configurations have demonstrated the intracellular delivery of Cre recombinase protein,[18b] and antibodies against cytoskeletal proteins.[18a]

Despite successful delivery of a broad variety of biomolecules into diverse cell types, the exact mechanism of whether and how the NW arrays can mechanically pierce cellular membranes and/or the nucleus is still not well understood, and has been the subject of an ongoing debate for almost a decade.[23] Various reports have demonstrated that NW-mediated intracellular delivery often relies on mechanical penetration, which can be maximized by manipulating a combination of key parameters, such as application of external force,[24] interfacing approaches,[13f,25] cellular adhesion force,[9a,26] NW geometry (density, length, and diameter),[17b,27] surface functionalization,[28] and interfacing time.[29] For example, effective delivery of biomolecules (plasmid DNAs, siRNAs, and proteins) into smaller immune cells that grow in suspension requires the use of longer (2–3 µm), sharper (diameter < 150 nm), and denser (0.3–1.0 NWs µm^{-2}) NWs, whereas slightly shorter and less dense NWs are more suitable for larger adherent cells.[17b] Arguing against NW-mediated direct penetration, some work has posited that the majority of NWs fail to gain a stable access to the cell interior spontaneously,[10a,29,30] and others have suggested that endocytosis could be one of the prevalent mechanisms

behind NW-mediated intracellular delivery.[23a] In particular, recent studies have shown evidence that vertical nanostructures induce well-defined membrane curvatures, stimulating clathrin-mediated endocytosis (CME) and caveolae-mediated endocytosis (CavME).[23a,31] Indeed, the endocytic process may occur when the NW diameter perceived by the cell is 50–100 nm, which is within the right size range for receptor-mediated endocytosis.[32]

Here, we used conical SiNW arrays (NW average dimensions of length 3.2 µm, diameter 100 nm, and density 0.3 NWs µm^{-2}; Figure S1a, Supporting Information) to achieve nucleic acid transfection into nonadherent cell lines (L1.2, mouse immune B; Jurkat, human CD4+ T) and adherent cell lines (GPE86, mouse embryonic fibroblast), as well as primary mouse immune T cells. Using flow cytometry, we examined the transfection efficiency by tracking the fluorescence-tagged plasmids and expression of reporter GFP within the cells detached from SiNWs; up to 25.4 ± 5.3% of L1.2 cells began to express GFP within 48 h. Relatively high transfection efficiency (30.7 ± 2.2%) was also achieved into difficult-to-transfect primary mouse T cells via SiNWs, especially in the absence of T cell receptor (TCR) stimulation. By combining confocal microscopy and focused ion beam scanning electron microscopy (FIB-SEM) imaging, we demonstrated that conical SiNWs induce direct penetration and enhanced CavME, facilitating uptake of plasmids.

2. Results and Discussion

2.1. Cell–SiNW Interface

The interplay between substrate topography and cellular behavior is complex and not fully described. A better characterization and understanding of the cell–SiNW interface is pivotal in maximizing SiNW-mediated delivery efficacy, via mechanical transfection. To study the interfacial interactions of cells with ordered SiNWs, we examined three cell types: GPE86, L1.2, and Jurkat cells (**Figure 1**
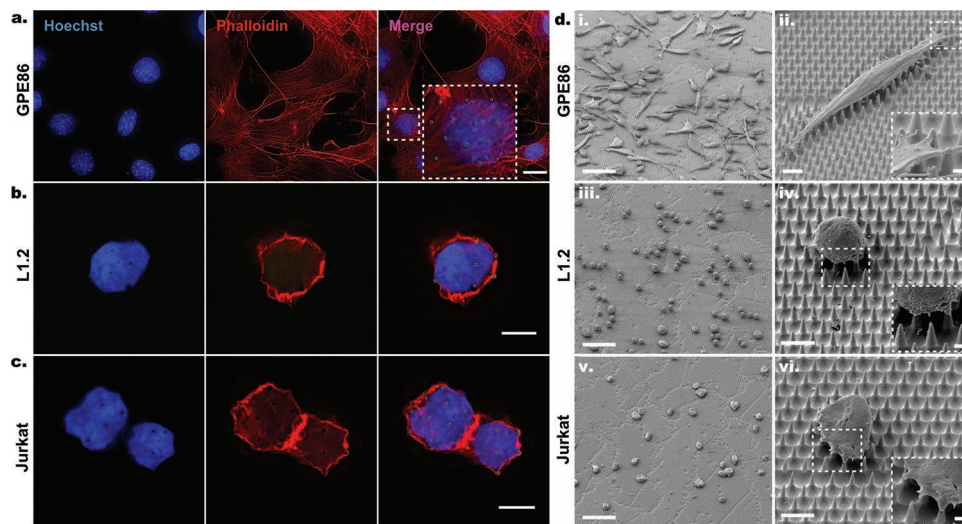
Figure 1. Cell–SiNW interface. a–c) Confocal imaging of fluorescence-stained a) GPE86, b) L1.2, and c) Jurkat cells after centrifugation and 6 h incubation on SiNWs. Cells were fixed and stained with phalloidin to reveal the F-actin (red), and Hoechst to reveal the nuclei (blue). White circles in the merged images indicate the positions of SiNWs inside the cells. Inset (merge column, a) is an enlargement (× 3) of the area outlined in the main image. Scale bars, a) 10 µm and b,c) 5 µm. d) SEM imaging showing zoom-out and zoom-in tilted (45°) views of i,ii) GPE86, iii,iv) L1.2, and v,vi) Jurkat cells on SiNWs after 6 h incubation. Scale bars, i,iii,v) 50 µm, ii,iv,vi) 5 µm, and 1 µm for the insets.

and Figure S1b–d, Supporting Information). Substrates were coated with positively charged poly-D-lysine (PDL). Such adhesion-mediating molecule coating serves a twofold purpose: to promote cell adhesion and to bind plasmid DNA (Figure S2, Supporting Information). All three cell types were seeded onto PDL-treated substrates. We applied controlled external force via centrifugation-induced gravity (200 g, ≈3.92 nN, 32 °C, 15 min), to facilitate intracellular interaction and efficient cytosolic delivery across the cell membrane barrier.[13b,25] After 6 h incubation, all three cell types were fixed and stained with fluorescence markers (phalloidin for F-actin, cytoskeletal filamentous actin; and Hoechst for the nuclei) to assess the cell–SiNW interface via confocal florescence microscopy (Figure 1a–c) and SEM (Figure 1d).

Cellular adhesion is considered a crucial process for development and maintenance of a functional cell–SiNW interface, which has been reported to promote cell penetration.[32a] Figure 1a–c is representative fluorescence confocal images demonstrating the forcible interfacing achieved between SiNWs and a) GPE86, b) L1.2, and c) Jurkat cells. The individual SiNW elements appear as black dots within all three cell types (marked as white circles in merged channel), indirectly suggesting the assisted impalement of SiNWs into the cell body (nucleus and cytoplasm) by applied centrifugal force. Multiple SiNWs were noted to interact with each cell type (Figure 1a–c, merged channel). In parallel, selected tilt-view SEM images illustrate the cellular morphology and adhesion of the plated cells on the conical SiNWs (Figure 1d). Adherent GPE86 cells displayed mainly a flattened and more elongated morphology, generating long lamellipodia with filopodial protrusions anchored on the tips of SiNWs (Figure 1d-ii). Short lamellipodia with filopodial protrusions were also observed on suspension-type Jurkat cells (Figure 1d-vi), whereas L1.2 cells largely maintained their globular shape (Figure 1d-iv). These findings are in agreement with previous study showing that cellular morphology and adhesion on NWs vary across different cell types.[17b]

The number of parameters in play at the cell–SiNW interface, and their complex and dynamic interactions, present a key challenge in delineating how decisions of cell behavior such as cell morphology, cytoskeleton arrangement, focal adhesion formation, motility, and other cellular processes are orchestrated. For example, focal adhesions have long been speculated to play a central role in cellular migration and regulation of both mechanical[33] and biochemical signaling pathways.[34] To better understand the cell proteins and complexes that participate in focal adhesion on SiNWs, we examined the distribution of F-actin, β-integrin (transmembrane receptor), and vinculin (membrane-cytoskeletal protein), which are reported to play important roles in mediating cell adhesion to the extracellular matrix.[35] **Figure 2**a–c displays the fluorescence staining of GPE86, L1.2, and Jurkat cells cultured on SiNWs. Interestingly, GPE86 cells on SiNWs formed ring-shaped adhesion complexes, assembled mainly by vinculins rather than F-actin or β-integrin (Figure 2a), which were absent in cells on flat Si (Figure S3, Supporting Information). Increased vinculin clustering indicates the potential for creating strong focal adhesion of GPE86 cells on the SiNWs substrate. Our observation of long lamellipodia with filopodial protrusions along SiNWs in SEM (Figure 1d-ii) supports this view. For L1.2 cells, vinculins were observed to be colocalized with the multilobed nucleus. While F-actin was found across the whole

cell, it was mainly the transmembrane receptor β-integrin that accumulated along the short filopodial protrusions (Figure 2b), facilitating the adhesion of L1.2 cells on SiNWs. Similar small "feet" made by β-integrins were also found on the cell surface of Jurkat cells, whereas vinculins were mainly distributed in the perinuclear region and F-actin accumulated at the membrane site (Figure 2c). Formation of small β-integrin protrusions on L1.2 and Jurkat cell surfaces, instead of ring-shaped vinculin complexes around the SiNWs, at least partially explains why suspension cells largely maintain globular shape and are less embedded onto SiNWs compared with their adherent counterparts.

To further investigate the alterations of cell focal adhesions over an extended period and their influence on cell motility on SiNWs, we performed confocal live cell imaging to record the migration trajectory of all three cell types on SiNW substrates (Figure 2d–f and Videos S1–S3, Supporting Information) over 30 h. The mean migration lengths of GPE86, L1.2, and Jurkat cells on SiNWs were 117.7, 62.4, and 79.0 µm, respectively; but no significant difference in cell mobility was observed compared with their counterparts on flat Si (Figure 2g). The longer migration lengths of GPE86 cells compared with L1.2 and Jurkat cells, are highly likely to be associated with their strong adhesion on SiNWs, which is mediated by focal adhesion molecules, especially vinculins. By binding to F-actin and modulating other focal adhesion molecules, such as integrins and talins, vinculins are involved in multiple steps during cell migration, including generation of traction forces and directional migration of cells.[36] Interestingly, though some nuclei of GPE86 cells moved little, their cell membrane displayed high levels of fluidity and plasticity, as evidenced by the creation of long and diverse protrusions at different orientations along the SiNWs (Video S4, Supporting Information).

The results show the development of a functional cell–SiNW interface, where the cells can form focal adhesions on SiNWs within 6 h after plating and exhibit cell motility over 30 h. This functional and sustainable interface sets the stage for the SiNW-mediated intracellular delivery.

2.2. Cellular Deformations Induced by SiNWs Promote Direct Penetration and Endocytosis

Direct intracellular delivery of biomolecules into the cells offers the advantage of bypassing inherent physical barriers including the cell membrane, actin cytoskeleton, endo-lysosomal entrapment, and cytosolic sequestration, as well as metabolic degradation, all of which normally reduce the efficiency of the exogenous cargo delivery.[37] As highlighted earlier, the question of whether NWs can directly penetrate through the 4–6 nm lipid bilayer—a challenging physical barrier that prevents most external species from accessing the cytosol—has been intensely debated. To reveal the actual types of interaction at the cell–SiNW interface, we used two complementary characterization techniques: confocal microscopy and FIB-SEM imaging.

We labeled the SiNWs with a fluorescent dye (fluorescein isocyanate; FITC), making the NWs visible under the confocal microscope. GPE86, L1.2, and Jurkat cells were seeded onto the FITC-labeled SiNWs. After short-term centrifugation and 6 h incubation, cells were fixed and stained with Hoechst and phalloidin, representing the nucleus and F-actin, respectively.
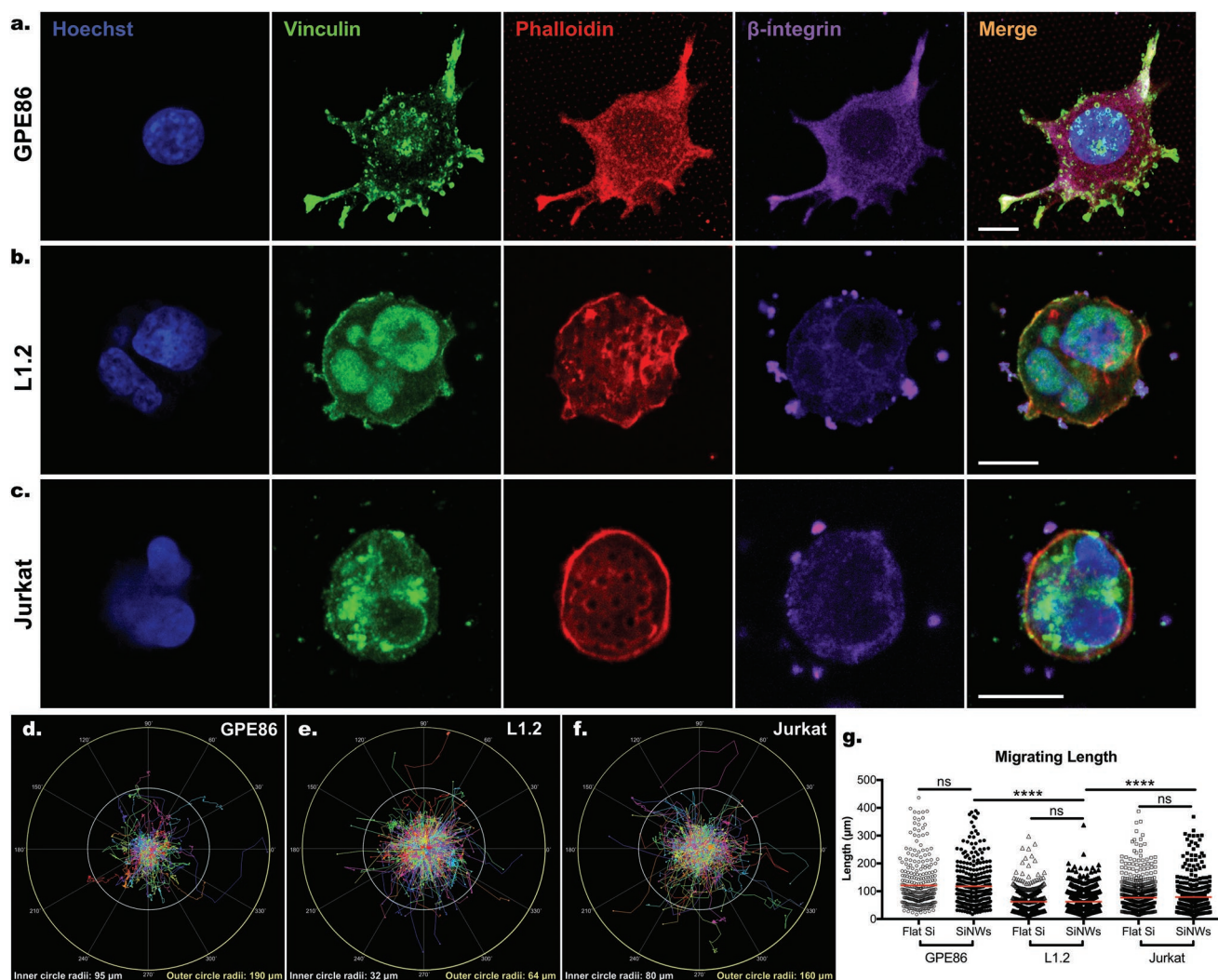
Figure 2. Cell focal adhesion formation and migration on SiNWs. a–c) Confocal imaging of fluorescence-stained a) GPE86, b) L1.2, and c) Jurkat cells after 6 h incubation on SiNWs. Cells were stained with Hoechst (blue) to reveal the nuclei, and vinculin (green), phalloidin (red), and β-integrin (purple) to reveal the cytoskeleton and focal adhesion points on the substrates. Scale bars, 10 µm. d–f) Polar plots showing the migration trajectory of d) GPE86, e) L1.2, f) Jurkat cells on SiNWs over 30 h. Sequential confocal images were taken every 10 min. Each curve in color represents the trajectory, including heading and length, of a single cell migrating from their origin. g) Graph plotting of the migration lengths (mean shown in red) of all three cell types on flat Si and SiNWs. Each symbol represents the migration length of one single cell ($N > 200$). ns, not significant ($p > 0.05$), ****$p < 0.0001$ (one-way ANOVA).

Figure 3 and Video S5 in the Supporting Information are 3D and 2D slice views of the compiled z-stack confocal images; they show reorganization of the actin cytoskeleton of a GPE86 cell at the SiNW sites (this is revealed by the absence of phalloidin staining in the corresponding positions of SiNWs that are illustrated in white). Similar results were obtained for the L1.2 (Figure S4a,b, Video S6, Supporting Information) and Jurkat (Figure S4c,d, Video S7, Supporting Information). The activity of actin has been correlated with endocytosis and subsequent cellular uptake of biomolecules.[38] However, due to practical limitations[39] of confocal microscopy, we are not able to draw more far-reaching conclusions regarding the precise biointerfacial interaction.

We used FIB-SEM imaging as a complementary method to unveil more details of the cell–SiNW interface at a higher nanoscale resolution. As SiNW-induced penetration can occur in the early stages of interfacing,[30a] and membrane self-resealing is likely to take place over a relatively short time-frame,[40] we performed this study after 1 h incubation of cells on SiNWs. FIB milling and SEM imaging were performed either at 90° or at 45° (Figure S5, Supporting Information) to the sample surface to investigate the cell–SiNW interface from different perspectives. **Figure 4**a illustrates two distinct patterns of how SiNWs interact with GPE86 cells. An individual SiNW is shown to breach the cell membrane and further indent the nucleus (Figure 4a-i); the second SiNW is engulfed by a continuous intact plasma membrane, accompanied by increased membrane curvatures (red arrows), similar to clathrin-coated pits and caveolae reported in recent studies (Figure 4a-ii).[23a,31] Figure 4b manifests SiNW insertion into the cytoplasm of a

ADVANCED
SCIENCE NEWS
www.advancedsciencenews.com

NANO · MICRO
small
www.small-journal.com
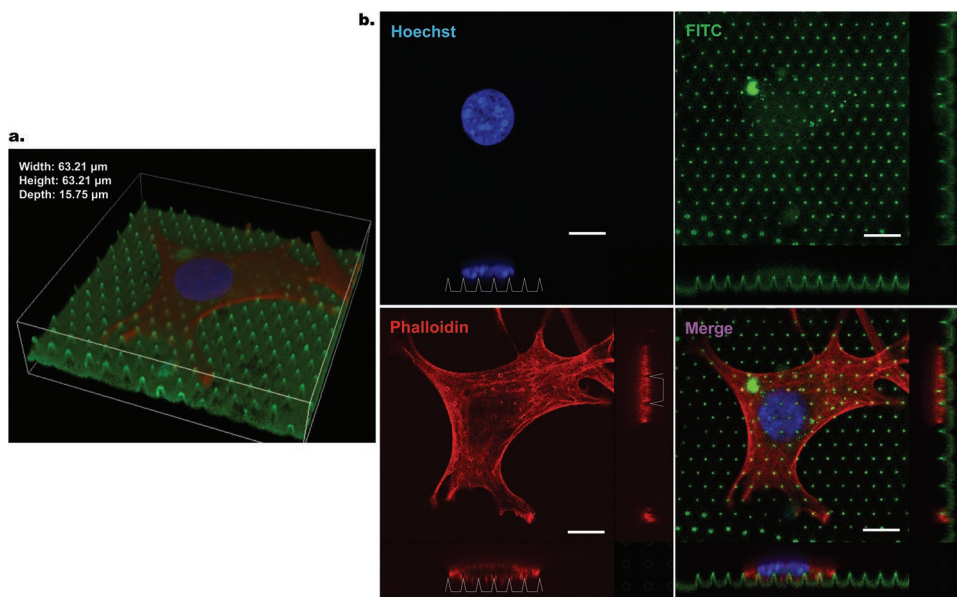
Figure 3. Membrane perturbation and nuclear deformation induced by conical SiNWs. a) 3D and b) slice view of confocal imaging of GPE86 cells on FITC (green)-labeled SiNWs after 6 h incubation. Cells were fixed and stained with phalloidin (red) and Hoechst (blue). SiNWs are depicted in white in (b) to represent their interaction with cell membrane and the nucleus. Scale bar, 10 µm.

L1.2 cell; Figure 4c displays the curving plasma membrane of Jurkat cells, with accumulation of multiple membrane invaginations and endocytic vesicles (red arrows) along the SiNWs. Sequential SEM imaging of the FIB sectioning at 45° provides additional insights into the cell–SiNW interactions. Figure 4d-i and Video S8 in the Supporting Information show clear evidence that the SiNWs (yellow arrow) directly penetrate into both the cytoplasm and nucleus of the L1.2 cell. By contrast, Figure 4d-ii and Videos S9 and S10 in the Supporting Information demonstrate that most SiNWs (yellow arrow) were engulfed by the intact cell membrane of the Jurkat cell.

The observations by both confocal and FIB-SEM suggest that direct penetration through membrane and nucleus might not be the prevalent, at least not the only, mechanism behind SiNW-mediated intracellular delivery. To understand whether other mechanisms, such as endocytosis,[23a,31] are involved, we investigated the role of two endocytic markers: clathrin heavy chain (CHC), a clathrin coat protein involved in CME; and caveolin-1 (CAV-1), a key protein for CavME. Plasmids tagged with a Cy3 fluorescence dye (Cy3-gWiz-GFP) were coated onto flat Si and SiNWs. Confocal microscopy images demonstrate the distribution of CAV-1 and CHC within GPE86 cells after 6 h interfacing with plasmid-coated flat Si (Figure 4e-i) and SiNWs (Figure 4e-ii). Compared to the random localization of CAV-1 in all three cell types on flat Si, CAV-1 was highly colocalized with Cy3-gWiz-GFP plasmids coated on SiNWs (Figure 4e and Figure S6, Supporting Information). But in contrast with a recent study,[23a] the clustering of CHC around SiNWs was less obvious than for CAV-1. Caveolae have been reported as a physiological membrane reservoir that quickly accommodates sudden and acute mechanical stress.[41] Combined with FIB-SEM imaging showing the membrane curvatures along SiNWs (Figure 4a,c), our results suggest that caveolar bulbs could accumulate during SiNW interfacing, which attenuates the increase
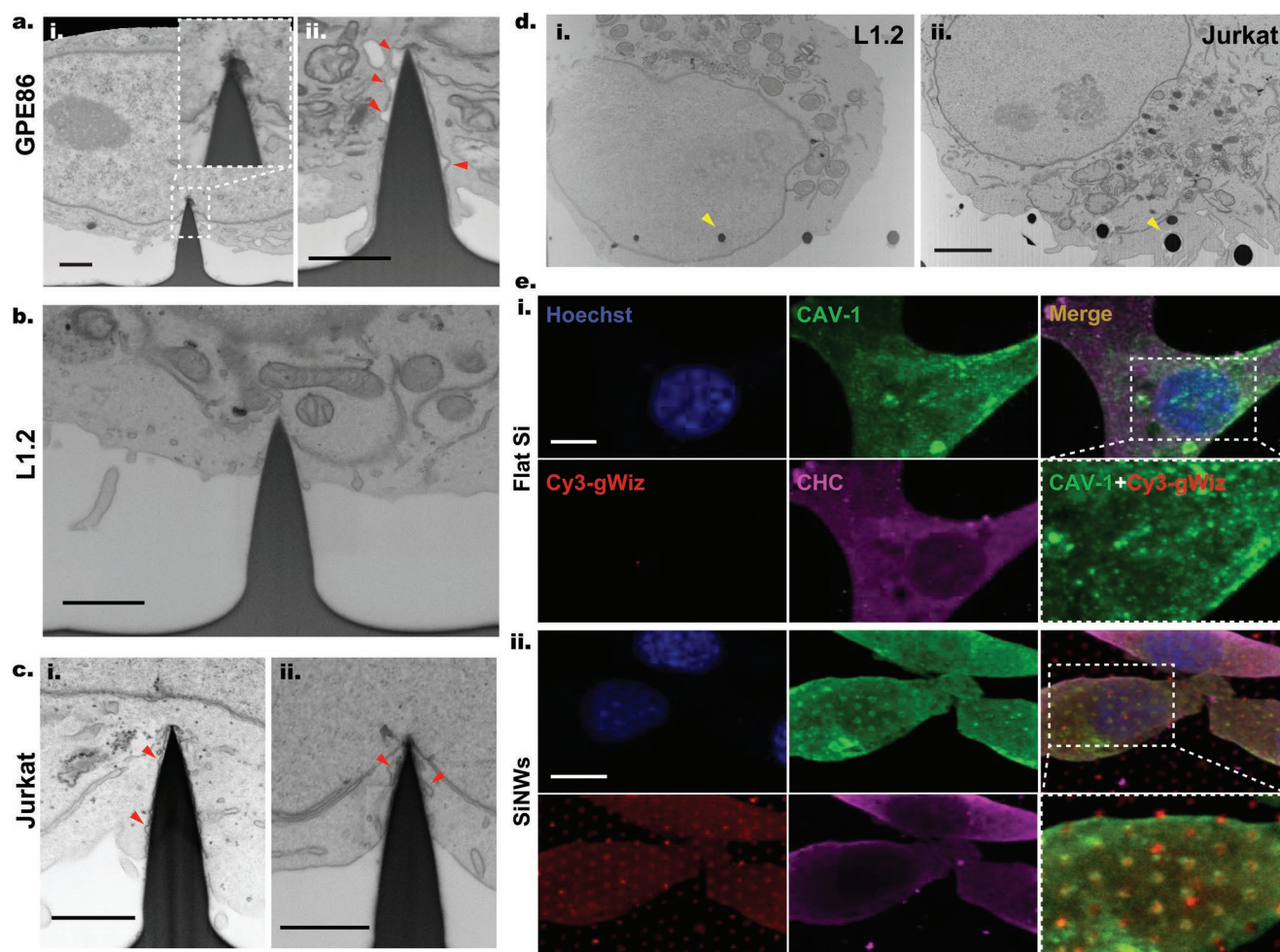
in membrane tension and protects the plasma membrane from rupture.[42] Caveolae are potential players enabling CavME and downstream cell signaling during cell–SiNW interaction.[31,43]

Overall, the results demonstrate that conical SiNWs are able to induce cellular deformations, which promote both direct membrane penetration and endocytosis (CavME). These two mechanisms may synergistically facilitate SiNW-mediated biomolecular uptake.

2.3. Minimal Impact on Cell Viability and Proliferation Induced by Conical SiNWs

Despite the efficient delivery of various biological molecules into cells using NWs,[17a,22,44] it is essential to prove that cells detached from SiNWs maintain high viability and proliferative capacity—prerequisites for potential application in cell-based immunotherapy. We followed the viability of cells cultured on SiNWs and tracked their proliferation up to 3 days after detaching from SiNWs.

By live/dead (fluorescein diacetate (FDA)/propidium iodide (PI)) staining, we observed neglectable difference in the viability of GPE86, L1.2, and Jurkat cells, in situ on flat Si and SiNWs after 6 h incubation (Figure S7, Supporting Information). To investigate whether unexpected damage would be introduced to cells due to extended SiNW-interfacing period and/or detachment process, we used the staining of annexin V-FITC/PI, to probe apoptosis/necrosis pathways[45] within detached cells at different time points. For example, Jurkat cells were harvested from flat Si and SiNWs after 2, 6, 12, and 24 h incubation. Flow cytometry results (**Figure 5**a,b) showed that over 95% of Jurkat cells maintained viability (annexin V^-/PI^-) after 2, 6, and 12 h culture on both SiNWs and flat Si, with less than 5% becoming apoptotic (annexin V^+/PI^-); this was consistent

**ADVANCED
SCIENCE NEWS**
www.advancedsciencenews.com

NANO · MICRO
small
www.small-journal.com

Figure 4. Cellular deformations and endocytosis induced by SiNWs. a–c) SEM images after FIB milling at 90° demonstrating the interface of a) GPE86, b) L1.2, and c) Jurkat cells with SiNWs (membrane curvatures indicated by red arrows). Inset in (a-i) is an enlargement (×3) of the area outlined in the original figure. d) SEM images after FIB milling at 45° revealing the SiNW (indicated by yellow arrows) penetration into the nucleus and cytoplasm of i) an L1.2 cell as well as the ii) engulfment of SiNWs by the cell membrane of a Jurkat cell. e) Representative confocal images showing the localization of nucleus (blue), caveolin-1 (Cav-1, green), and clathrin heavy chain (CHC, magenta) within GPE86 cells cultured on i) flat Si and ii) SiNWs, which were coated with Cy3-gWiz-GFP (Cy3-gWiz, red) plasmids. The bottom right images in (i,ii) are enlargements (×2) of the areas outlined in "Merge," showing Cav-1 and Cy3-gWiz channels. Original images a–d) are black–white inverted. Scale bars, a–c) 1 µm, d) 2 µm, and e) 10 µm.

with the viability result achieved by in situ live/dead (FDA/PI) staining (Figure S8, Supporting Information). After 24 h incubation, the population of dead/necrotic cells (annexin V$^+$/PI$^+$) remained negligible, $0.83 \pm 0.1\%$ and $0.74 \pm 0.2\%$ on flat Si and SiNWs, respectively, indicating that SiNWs did not induce necrotic cell death of Jurkat cells. Annexin V$^+$/PI$^-$ population rose up to 10% for cells on SiNWs, more than double of that on flat Si, suggesting a likely increased apoptosis due to prolonged SiNW-interfacing. Yet, the possibility of SiNW-enhanced lipid scrambling[17a] cannot be ruled out, as annexin V is also a crucial protein in the active process of membrane remodeling.[46] By measuring apoptosis-related caspase 3/7 activity, we confirmed that SiNWs did not induce significant increase in apoptotic cell population (Figure S9, Supporting Information).

To examine the proliferative capacity post NW-culture, GPE86, L1.2, and Jurkat cells were first labeled with a proliferation tracking dye, CellTrace Violet (CTV),[47] before seeding

onto SiNWs. After 6 h incubation, the cells were detached from SiNWs either by trypsinization (GPE86) or gentle pipetting (L1.2 and Jurkat). Harvested cells were then cultured back in fresh media and analyzed by flow cytometry on Days 2 and 3. Because CTV covalently binds to intracellular proteins in the cytoplasm and nucleus, and halves in amount with each round of cell division,[48] the proliferation rate of cells is negatively correlated with CTV fluorescence intensity. CTV unstained cells (CTV$^-$) and CTV stained cells (CTV$^+$, fixed in fluorescence-activated cell sorting (FACS) buffer after 6 h incubation) worked as negative and positive controls, respectively.

Among the three cell types, L1.2 cells were most prolific on Days 2 and 3, indicated by their lower CTV fluorescence intensity (Figure 5c). On Day 3, CTV intensity in L1.2 cells was reduced almost to the level of the negative control. Although CTV reduction of L1.2 cells harvested from SiNWs lagged

ADVANCED
SCIENCE NEWS
www.advancedsciencenews.com

NANO · MICRO
small
www.small-journal.com
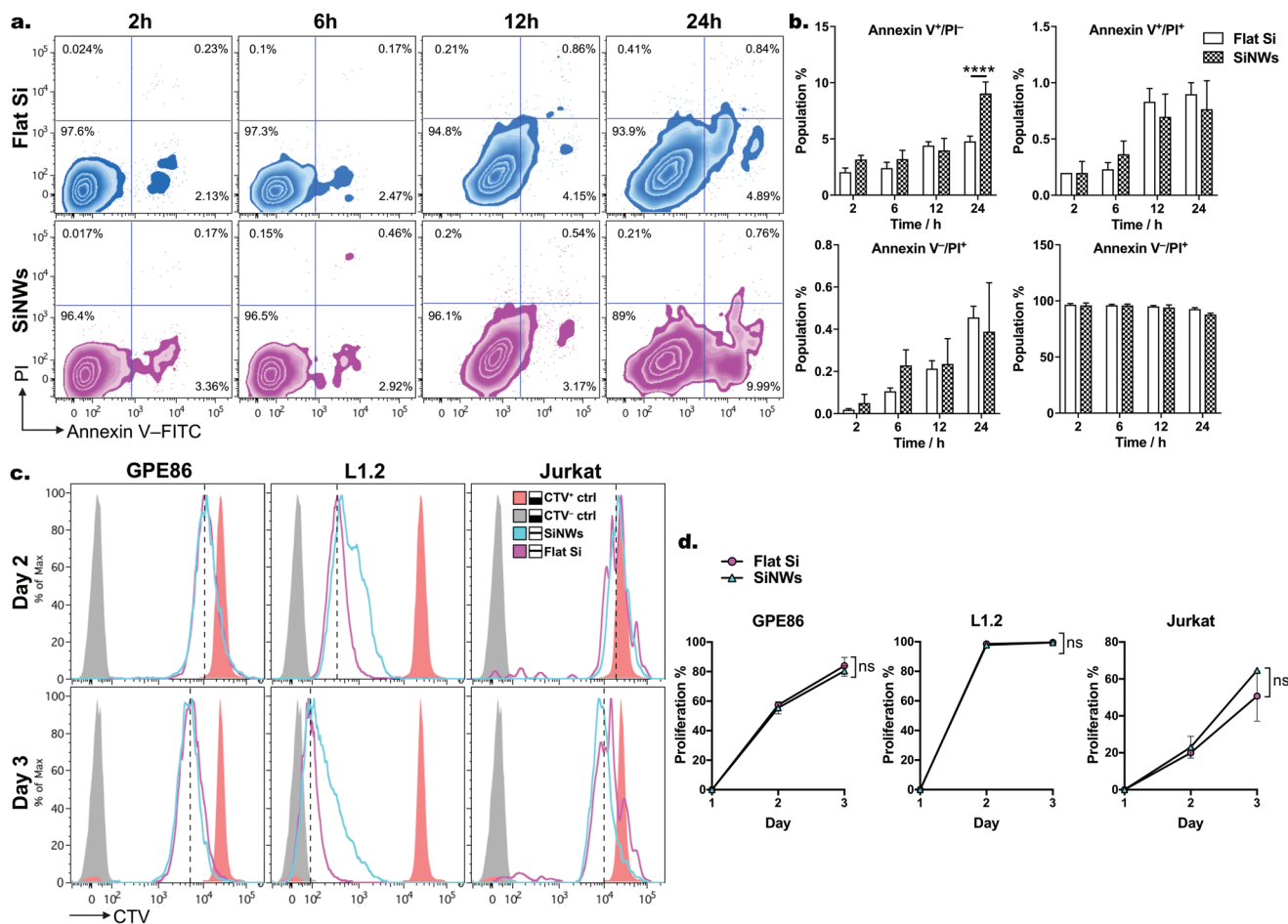
Figure 5. Cell apoptosis and proliferation after detachment from SiNW substrates. a) Flow cytometry of Jurkat cells harvested from flat Si and SiNWs at different incubation times (2, 6, 12, and 24 h), and stained with annexin V-FITC/PI Apoptosis Kit. Gating strategy showing four populations (annexin V⁻/PI⁻, annexin V⁺/PI⁻, annexin V⁺/PI⁺, and annexin V⁻/PI⁺). b) Statistical analysis of the percentages of the four populations (annexin V⁻/PI⁻, annexin V⁺/PI⁻, annexin V⁺/PI⁺, and annexin V⁻/PI⁺) after detachment from flat Si and SiNWs at different incubation times as in (a). c) Expression of CTV in GPE86, L1.2, and Jurkat cells on Days 2 and 3 after detachment from 6 h incubation on flat Si (magenta curve) and SiNWs (blue curve). Unstained cells (solid gray) and CTV freshly stained cells (solid red) served as negative and positive controls, respectively. d) Quantification of the proliferation rate of cells harvested from flat Si and SiNWs as shown in (c). ns, not significant ($p > 0.05$), ****$p < 0.0001$ (two-way ANOVA).

slightly compared with that from control flat Si, the percentage of cells undertaking proliferation was very similar for both substrates (99.5 ± 0.1%; Figure 5d). On Day 2, GPE86 cells demonstrated less CTV reduction and therefore reduced proliferation (56.4 ± 2.8%) compared with L1.2 cells. But CTV intensity dropped continuously from Days 2 to 3, indicating ongoing proliferation (reaching 80.5 ± 3.6% on Day 3). No significant difference was observed in CTV reduction and proliferation rate between GPE86 cells harvested from SiNWs and flat Si. Jurkat cells showed the lowest proliferation rate. But similar to GPE86 cells, the CTV intensity of Jurkat cells continued to decrease from Days 2 to 3, with the proliferation percentage increasing from 23.0 ± 5.8% to 64.6 ± 0.4%.

These results confirm our hypothesis that conical SiNWs induce minimal necrosis and negligible apoptosis for up to 12 h. Cells can be retrieved from SiNWs while maintaining similar proliferative capacity as their counterparts on flat Si. Yet caution should be applied when culturing cells on SiNWs for over 24 h, since the rate of apoptosis might increase.

2.4. SiNWs Mediate Transfection of Plasmids into Immortalized Cell Lines

Having demonstrated that conical SiNWs induce membrane disruption and nuclear perturbation, while preserving cell viability and proliferative capacity after harvesting from the SiNWs, we tested delivery of plasmids into all three cell lines. Previous studies have used vertical SiNWs to transfect biomolecules (including DNAs, RNAs, peptides, and proteins) into a variety of cell types with high efficiency.[16b,17a,b,22,44] Some of those results relied on fluorescence microscopy imaging to measure the expression of reporter genes (e.g., plasmids encoding GFP)[16b] and fluorescence tagged cargoes (e.g., Cy5-labeled plasmids and Alexa 546-labeled siRNA)[17a] within the transfected cells in situ (on the NW substrates).

Instead, here we used flow cytometry technique to detect the fluorescence in the transfected cells detached from SiNWs. This enables more sensitive, objective, rapid, and reproducible measurement compared with fluorescence microscopy
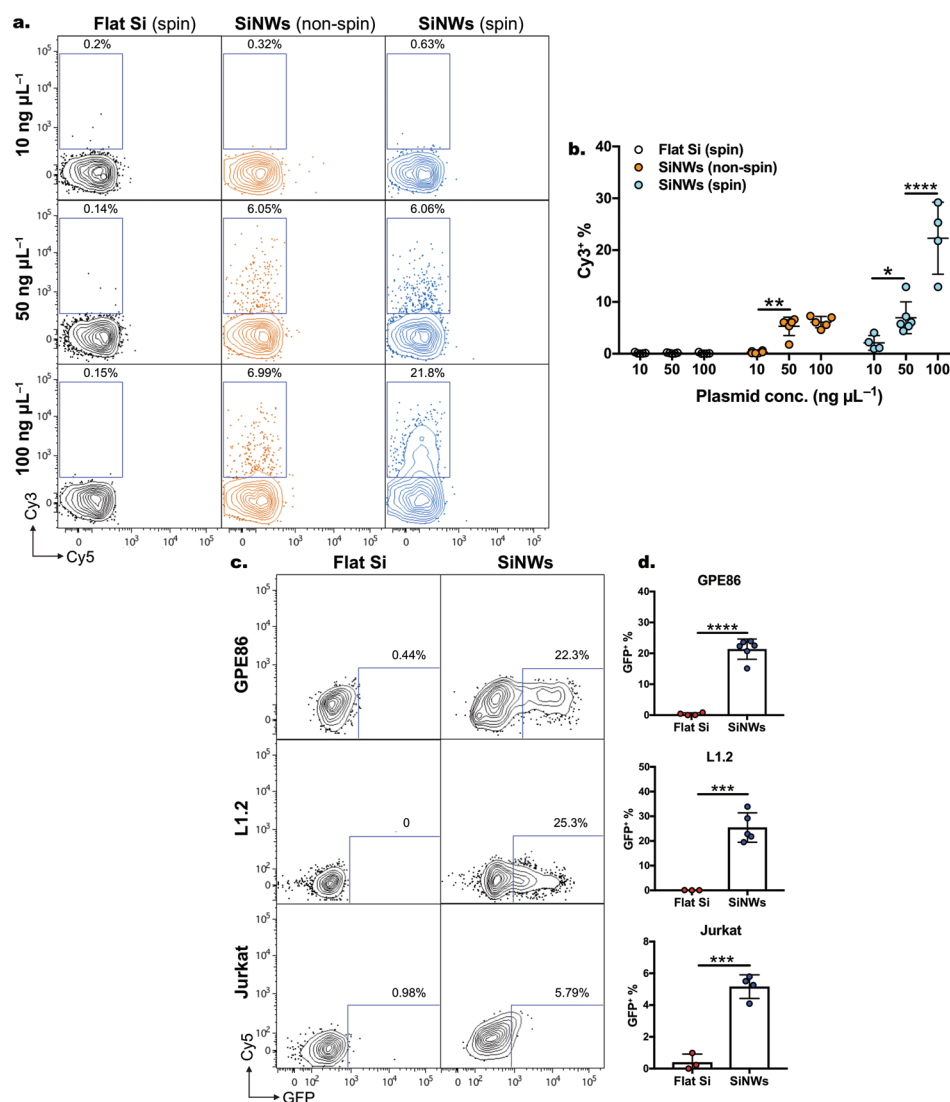
Figure 6. Plasmid insertion and cell transfection by flat silicon substrates and SiNWs. a) Flow cytometry of L1.2 cells harvested after 6 h incubation on flat Si (with spin), SiNWs (without spin), and SiNWs (with spin), coated with Cy3-gWiz-GFP plasmids at different concentrations (10, 50, and 100 ng μL^{-1}). Numbers adjacent to outlined areas indicate the percentage of Cy3$^+$ cells (indicative of plasmid insertion). b) Percentages of Cy3$^+$ L1.2 cells as shown in (a). Black, orange, and blue dots indicated cells harvested from flat Si (spin, black dots), SiNWs (nonspin, orange dots), and SiNWs (spin, blue dots), respectively. *$p = 0.0104$, **$p = 0.003$, ****$p < 0.0001$ (two-way ANOVA). c) Flow cytometry of GPE86, L1.2, and Jurkat cells 48 h after harvesting from plasmid-coated flat Si and SiNWs (with 6 h incubation). Numbers adjacent to outlined areas indicate the percentage of GFP$^+$ cells (indicative of positive transfection). d) Percentage of GFP$^+$ cells harvested from flat Si (red dots) and SiNWs (blue dots) as in (c). ***$p = 0.0002$, ****$p < 0.0001$ (Mann–Whitney's U-tests). Each symbol b,d) represents an individual substrate.

imaging. We added Cy3-tagged plasmids (Cy3-gWiz-GFP) onto flat Si and SiNWs at three distinct concentrations: 10, 50, and 100 ng μL^{-1}. L1.2 cells were seeded onto the substrates, with or without the application of centrifugal external force. Cells were incubated for 6 h before detaching from the substrates by gentle pipetting. Harvested cells were stained with Hoechst and PI, and analyzed by means of flow cytometry to measure the Cy3 intensity within viable (Hoechst$^+$/PI$^-$) population (**Figure 6**a,b). The results showed no Cy3$^+$ population in L1.2 cells cultured on flat Si, demonstrating no plasmid insertion at all three tested concentrations. But for L1.2 cells cultured on SiNWs coated with plasmids at 10 and 50 ng μL^{-1}, we observed an increase in Cy3$^+$ population from 0.3 ± 0.2% to 5.3 ± 1.8%.

When exposed to further increased plasmid concentration (from 50 to 100 ng μL^{-1}), no further enhancement in plasmid uptake was observed in L1.2 cells settled on SiNWs by gravity alone (Figure 6a center,b). By contrast, when applying external centrifugal force to strengthen the cell–SiNW interaction, the percentage of L1.2 cells gaining Cy3-tagged plasmids rose more than three times from 6.9 ± 3.1% for 50 ng μL^{-1} to 22.3 ± 7.0% for 100 ng μL^{-1} (Figure 6a right,b).

After validating the SiNW-mediated plasmid insertion into L1.2 cells, as well as GPE86 and Jurkat cells (Figure S10, Supporting Information), we investigated the efficiency of reporter gene expression by measuring the GFP intensity. GPE86, L1.2, and Jurkat cells were cultured on flat Si and SiNWs coated

with untagged plasmids (gWiz-GFP). After centrifugation and 6 h incubation, cells were harvested from the SiNWs, returned to fresh media, and cultured for another 48 h to allow for the expression of GFP. We performed flow cytometry analysis to determine the fluorescence intensity of GFP within these cells. Corresponding to the null plasmid insertion described above, control flat Si rendered no GFP+ population for any of the three cell types (Figure 6c,d). For cells harvested from SiNW-mediated transfection, L1.2 cells exhibited the highest transfection efficiency, with 25.4 ± 5.3% GFP+ population, followed by GPE86 cells, with 21.4 ± 3.3% and Jurkat cells, with only 5.2 ± 0.7%. The lower transfection efficiency in Jurkat cells might result from multiple factors. For example, FIB-SEM images (Figure 4c,d-ii) demonstrate that the Jurkat cell membrane mostly maintains its integrity, which may limit the amount of plasmid inserted by direct penetration through plasma membrane and the nucleus. Though endocytosis might take place, DNA degradation[49] and unsuccessful endosomal escape[50] can hamper GFP expression. In addition, the results of the proliferation study for Jurkat cells show that the slow recovery from SiNW culture may also contribute to their lower transfection efficiency.

2.5. SiNWs Mediate Delivery of Nucleic Acids into Primary Immune T Cells In Vitro

Retrovirus and lentivirus are generally used to transduce difficult-to-transfect primary immune T cells, and to induce their specific antitumor responses. But artefacts caused by open reading frame disruption and gene activation can be introduced into the host cells.[51] In addition, ex vivo TCR activation and sustained proliferation of activated T cells required for most efficient transduction may impair the half-life and repertoire, leading to exhaustion of transduced T cells.[52] Better methods need to be developed for genetic modification of T cells in vitro, to fully preserve their immunologic competence.

We have shown that conical SiNWs have the potential to transfect immortalized cell lines in a mechanical manner. To avoid the consequences of preactivation that is normally involved in conventional viral and nonviral transfection, we used SiNWs to transfect inactivated primary immune T cells and investigated their activation status after SiNW-interfacing (Figure S11, Supporting Information). Total T cells were isolated from wildtype mice and seeded onto flat Si and SiNWs coated with Cy3-gWiz-GFP plasmids. By detecting the Cy3 expression through flow cytometry, we determined that 32.8 ± 0.4% of primary mouse T cells obtained Cy3-gWiz-GFP plasmids from SiNWs after 6 h incubation, whereas less than 1% of Cy3+ T cells were observed from flat Si (**Figure 7**a,b). Importantly, the 6 h interfacing period caused almost no alteration to the expression level of key surface activation markers and major inflammatory cytokines within T cells harvested from SiNWs (Figure S12, Supporting Information). This indicates that the majority of T cells remained at naïve stage after SiNW-mediated transfection.

To further investigate the transfection efficiency in terms of GFP expression, we cultured T cells detached from flat Si
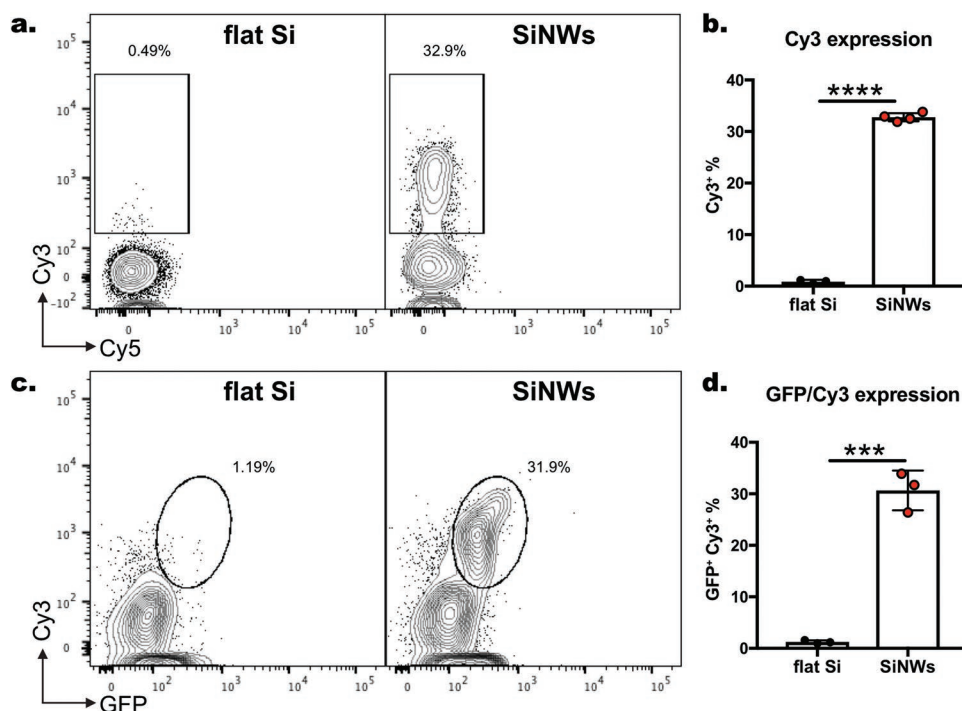
Figure 7. Transfection of Cy3-gWiz-GFP plasmids into inactivated primary mouse T cells. a) Flow cytometry detection of Cy3 expression within primary mouse T cells, detached from flat Si and SiNWs coated with Cy3-gWiz-GFP plasmids, after 6 h incubation. b) Quantification of the percentage of Cy3+ cells harvested from flat Si and SiNWs as in (a). c) Flow cytometry detection of Cy3 and GFP expression within primary mouse T cells 48 h after re-culture in fresh media. d) Quantification of the percentage of GFP+ Cy3+ cells harvested from flat Si and SiNWs as in (c). ***p = 0.0002, ****p < 0.0001 (Mann–Whitney's U-tests). Each symbol b,d) represents an individual substrate.

and SiNWs in fresh media for another 48 h. The result showed that 30.7 ± 2.2% of T cells harvested from SiNWs became Cy3$^+$ GFP$^+$, indicating the preservation of Cy3-gWiz-GFP plasmids within the transfected T cells and their expression of GFP reporter gene after 48 h (Figure 7c,d). These data are an important step toward the use of SiNWs to mediate delivery of gene constructs directly into inactivated primary T cells. This bypasses the prerequisite of TCR engagement, helping to maintain an intact immune competence.[53]

3. Conclusions

This study probed the biointerfacial interactions between conical SiNWs and diverse cell types, including immortalized adherent fibroblast (GPE86), suspension immune B (L1.2), and T (Jurkat) cells, as well as primary immune T cells. Cytoskeletal molecules such as vinculins play an important role in cell adhesion and migration on SiNWs. For example, in adherent GPE86 cells, vinculins accumulate along the lamellipodia and filopodial protrusions anchoring on the NW tips, promoting focal adhesion formation and membrane elongation on SiNWs, while in nonadherent L1.2 and Jurkat cells, vinculins mainly support the structure of the nucleus. The migration study showed that the motility of cells cultured on SiNWs is similar to that on flat Si. Importantly, we observed that the majority of cells detached from SiNWs retain their proliferative capacity—a key advance that will underpin development of significant biomedical applications.

6 h incubation of cells on plasmid-coated SiNWs was found to be sufficient for cell transfection while maintaining optimal cell viability. External centrifugal force can further enhance nucleic acid uptake, most likely through increased cellular deformations, which facilitate direct membrane penetration and endocytosis (CavME), as illustrated by confocal and FIB-SEM imaging. Transfection with GFP reporter (gWiz-GFP) plasmids through SiNWs yields 21.4 ± 3.3%, 25.4 ± 5.3%, and 5.2 ± 0.7% GFP$^+$ populations of GPE86, L1.2, and Jurkat cells, respectively. In the case of primary immune T cells, we achieved a repeatable > 30% gWiz-GFP transfection.

We demonstrated that freshly sorted inactivated T cells remain at a naïve stage after 6 h interfacing with SiNWs, and transfection required no pre-engagement of activation stimuli, which are applied in most viral and nonviral methods and may result in skewing of the TCR repertoire[54] and reduced alloreactivity.[55] Our results create an important avenue for ex vivo T cell modification that better preserves immunologic competency for antitumor immunotherapy. This better understanding of nanotopographical effects on cell function, particularly intracellular delivery, will help to guide the design of biomaterials and promote their application in cell therapies.

4. Experimental Section

Preparation of Si Wafers: Before polystyrene microsphere (PSMS, Polysciences, Inc.) deposition, flat silicon wafers (3″, p-type, 3–6 Ω cm, ⟨100⟩, Siltronix, France) were cut into quarter pieces and cleaned by sonication in 1:1 solution of ethanol:acetone for 5 min and then sonicated again in MilliQ water for 5 min. This was followed by dipping the wafer pieces into boiling Piranha solution (3:1 H$_2$SO$_4$:H$_2$O$_2$

v/v, 75 °C, Avantor Performance Materials) for 1 h to remove any organic contaminants, then washing with water and drying under a nitrogen jet.

Convective Assembly Deposition: Hexagonally close-packed PSMS monolayers were deposited over quarter pieces of a 3″ Si wafer by convective assembly. The apparatus included a mounted microscope slide that was used as a blade for the PSMS depositions, a 50 mm motorized translation stage (MTS50-Z8, Thorlabs, Inc.), and a compact sub-Hertz pendulum vibration isolation system (TMC). The blade was adjusted to leave a small space between the bottom edge of the blade and the Si substrate. 25 µL of a suspension of PSMS (polybead microspheres solutions, various diameters, 2.5% w/v in water) was injected into the space between the blade and the sample using a micropipette, forming a meniscus between the pinned substrate and the bottom edge of the blade. This resulted in a continuous contact line of PSMS suspension on the Si substrate. To deposit PSMS in a uniform monolayer, operating parameters such as stage velocity and PS suspension concentration were adjusted.

Oxygen Plasma Reactive Ion Etching (RIE) of Polystyrene Microspheres: Samples prepared by convective assembly were inserted into Plasmalab100 ICP380 deep reactive ion etcher (Oxford Instruments), where oxygen plasma treatment was performed in order to reduce the size of the PSMS. During the etching step, a flow rate of 100 sccm O$_2$ was used with inductively coupled plasma (ICP) power of 100 W and bias power of 50 W. The APC valve position was set at 35 and He pressure was set at 10 Torr. The reduced size PSMS served as a mask for the subsequent silicon etching in two steps.

Deep RIE of Silicon: 1) Bosch process: Silicon etching was performed by alternate cycles of passivation and etching steps to obtain SiNWs with a cylindrical profile. During the passivation step (6 s), a flow rate of 150 sccm C$_4$F$_8$ and 3 sccm SF$_6$ was used with ICP power of 1500 W and bias power of 5 W. During the etching step (8 s), a flow rate of 150 sccm SF$_6$ and 3 sccm C$_4$F$_8$ was used with ICP power of 2000 W and bias power of 20 W. The APC valve position was set at 70 and He pressure at 10 Torr in both steps. The etching depth of Si was controlled by the number of cycles. Following the Bosch process, PSMS were removed either by sonication of the samples in MilliQ water for 2 min or by performing oxygen plasma RIE with high power. In the case of sonication, samples were then dried under a nitrogen jet and inserted back to the deep reactive ion etcher. 2) Pseudo-Bosch process: Silicon etching was performed in a simultaneous flow of 100 sccm SF$_6$ and 40 sccm C$_4$F$_8$ at a pressure of 10 mTorr, with ICP power of 1500 W and bias power of 50 W to achieve a conically shaped profile of the SiNWs. He pressure was set at 10 Torr. The tip diameter and the final length of the SiNWs were controlled by etching time.

Surface Functionalization of SiNWs: Substrates were immersed in 70% ethanol and allowed to dry at room temperature (RT) for 2 h in a laminar flow cabinet. Following this, substrates were coated with 10 µL of PDL (Sigma-Aldrich) at the concentration of 167 µg mL^{-1} in H$_2$O. After 4 h incubation at 4 °C, excessive PDL solution was aspirated before nucleic acids loading.

Cell Culture: Four types of cell lines, GPE86 (ATCC, mouse embryonic fibroblasts), L1.2 (ATCC, mouse B cells), Jurkat (ATCC, human CD4$^+$ T cells), and primary mouse T cells (isolated from mouse lymph nodes, approved by Monash Animal Research Platform's Ethics Committee) were investigated in this study. GPE86 cells were grown and maintained in complete Dulbecco's modified Eagle's medium (DMEM (Gibco), supplemented with 10% fetal bovine serum (FBS, Gibco), 1 × 10^{-3} M sodium pyruvate, 2 × 10^{-3} M L-glutamine, 100 U mL^{-1} penicillin, and 100 µg mL^{-1} streptomycin (Gibco). L1.2 and Jurkat cells were grown and maintained in complete RPMI (RPMI-1640 (Gibco), consisting of 10% FBS, 10 × 10^{-3} M 4-(2-hydroxyethyl)-1-piperazineethanesulfonic acid, 1 × nonessential amino acids solution (Gibco), 1 × 10^{-3} M sodium pyruvate, 2 × 10^{-3} M L-glutamine, 100 U mL^{-1} penicillin, 100 µg mL^{-1} streptomycin, and 55 × 10^{-6} M 2-mercaptoethanol (Gibco)). Primary mouse T cells were grown and maintained in complete RPMI supplemented with or without anti-mouse CD3 (5 µg mL^{-1}), anti-mouse CD28 (5 µg mL^{-1}), and IL-2 (20 ng mL^{-1}). All cells were incubated at 37 °C with 5% CO$_2$.

FITC Labeling of SiNWs: Substrates were first ozone-cleaned (10 min), and then incubated in 2% v/v 3-aminopropyltrimethoxysilane (Sigma-Aldrich) in dry toluene (Sigma-Aldrich) in an orbital shaker for 10 min, RT. Substrates were rinsed three times with toluene and dried at 110 °C on a hot plate for 10 min. Silanized substrates were then immersed into freshly prepared solution of FITC (1×10^{-3} M in Dulbecco's phosphate-buffered saline (DPBS), Gibco). After 10 min incubation at RT, substrates were washed three times with DPBS and left to dry at RT.

Cell Fixation and Fluorescence Staining: Cells grown on the substrates were washed with DPBS and then fixed in a solution of 4% paraformaldehyde (Electron Microscopy Sciences) for 10 min, followed by permeabilization with 0.1% Triton X-100 (Sigma-Aldrich) in DPBS for 5 min at RT and washing three times with DPBS. Cells were blocked with 1% w/v bovine serum albumin (BSA, Sigma-Aldrich) solution for 1 h at RT and washed three times with DPBS. For primary antibody staining, cells were stained with Hoechst (Hoechst 33342, Sigma-Aldrich), Alexa Fluor 568 Phalloidin (Life Technologies), anti-vinculin monoclonal antibody (rabbit, Sigma-Aldrich), anti-β-integrin monoclonal antibody (mouse, Invitrogen), anti-caveolin-1 polyclonal antibody (rabbit, Abcam), and anti-clathrin heavy chain monoclonal antibody (mouse, Life Technologies), for 45 min, RT. After washing three times with DPBS, cells were then further stained with secondary antibodies, Alexa Fluor 488 chicken anti-rabbit IgG (Life Technologies) and Alexa Fluor 647 goat anti-mouse IgG (Life Technologies), for 30 min, RT. Cells were washed three times with DPBS and left in DPBS for confocal imaging.

Confocal Laser Scanning Microscopy: A Nikon A1R confocal laser scanning microscope system was used for fluorescence imaging. Hoechst, Alexa Fluor 488 chicken anti-rabbit IgG (indicating vinculin), Alexa Fluor 568 Phalloidin, and Alexa Fluor 647 goat anti-mouse IgG (indicating β-integrin) were excited at 340, 488, 578, and 647 nm, with emission at 510, 520, 600, and 670 nm, respectively. Observations were conducted at more than ten different locations on the surface of each sample at the magnification of 60 × water immersed objective lens. Images were analyzed using the Nikon NIS-Elements Advanced Research software provided by the manufacturer.

Live Cell Microscopy for Migration Study: 20 000 pR-GFP GPE86 cells were seeded (constitutively expressing GFP) onto substrates in 48-well plate, followed by centrifugation at 200 g, 32 °C, 15 min. After centrifugation, substrates carrying cells were transferred to a Nunc glass bottom dish (Thermo Fisher Scientific) with fresh complete DMEM and placed in the portable incubation chamber provided by the manufacturer, at 37 °C and 5% CO₂. GFP was excited using the 488 nm laser with low intensity, to avoid phototoxicity that might induce cell death, and detected at 513 nm. This was observed at magnification of 10 × objective lens. Confocal images were taken every 10 min over 30 h. Live cell images were analyzed using Nikon NIS-A Advanced 2D Tracking Module.

Sample Preparation for SEM Imaging: Cells grown on the substrates were rinsed with 0.1 M sodium cacodylate buffer (Electron Microscopy Sciences) and fixed with 2.5% glutaraldehyde (Electron Microscopy Sciences) in 0.1 M sodium cacodylate at 4 °C overnight. Following this, substrates were washed (3 × 5 min) with chilled 0.1 M sodium cacodylate buffer and post-fixed with 1% osmium tetroxide (Electron Microscopy Sciences) in 0.1 M sodium cacodylate at RT for 1 h. After repeating the washing step, substrates were gradually dehydrated with increasing concentrations of ethanol: 50%, 70%, 90% (1 × 10 min), and 100% (2 × 10 min) at RT, and were finally critical point dried (CPD 030 Critical Point Dryer, BAL-TEC). Substrates were then mounted on SEM stubs and sputter-coated with a thin layer of either gold or platinum in order to increase their conductivity.

Intracellular Compartments Staining: The sample preparation combined heavy metal staining with resin embedding. In particular, samples were rinsed with 0.1 M sodium cacodylate buffer and fixed with 2.5% glutaraldehyde in the same buffer at 4 °C overnight (4 h in the case of L1.2 and Jurkat cells). Following this, the samples were washed (3 × 5 min) with chilled 0.1 M sodium cacodylate buffer and quenched with chilled 20×10^{-3} M glycine solution (Sigma-Aldrich) in the same buffer for 20 min. After repeating the washing step, samples were post-

fixed by combining equal volumes of 4% aqueous osmium tetroxide with 2% potassium ferrocyanide (UNIVAR) in 0.2 M sodium cacodylate buffer on ice for 1 h. Samples were rewashed (3 × 5 min) with chilled buffer and incubated with 1% tannic acid (BDH) in water at RT for 20 min. After rinsing with buffer (2 × 5 min), samples were further incubated with 2% aqueous osmium tetroxide at RT for 30 min. Samples were washed (2 × 5 min) with distilled water and incubated with syringe-filtered 4% aqueous uranyl acetate (UNIVAR) at 4 °C overnight. Samples were washed (3 × 5 min) with chilled distilled water and gradually dehydrated with increasing concentrations of ethanol: 10%, 30%, 50%, 70%, 90%, and 100% (1 × 7 min) at RT. An epoxy-based resin 20 mL solution was prepared by initially mixing 12.2 g of DDSA (dodecenyl succinic anhydride specially distilled, Electron Microscopy Sciences), 4.4 g of Araldite (GY 502, Electron Microscopy Sciences), and 6.2 g of Procure 812 (EMBED 812 RESIN) using a mechanical stirrer. Once the solution was uniformly mixed, 0.8 mL of BDMA (N-benzyldimethylamine, Electron Microscopy Sciences) was added while stirring. Samples were infiltrated with increasing concentrations of the freshly prepared resin solution in 100% ethanol at RT and in a sealed container using the following ratios: 1:3 (3 h), 1:2 (3 h), 1:1 (overnight), 2:1 (3 h), 3:1 (3 h). Following this, samples were finally infiltrated with 100% resin solution overnight. After polymerization at 60 °C, the excess resin was drained away by mounting the samples vertically for 1 h.

SEM Imaging: SEM imaging was performed of both bare SiNWs and SiNW substrates with cells on a Nova NanoSEM 430 (FEI). The images were taken at tilted (45°) or top views with an electron beam acceleration voltage of 5 kV and a current of 0.11 nA, while using a secondary electron detector.

FIB Sectioning and Imaging: FIB sectioning of SiNW substrates with cells was performed using a Thermo Fischer Helios G4 UX FIB-SEM vertically and at 45° to the sample surface. Before FIB sectioning, the region of interest was protected from ion beam (i-beam) damage using i-beam assisted deposition of ≈0.5 µm thick platinum layer. The coating was carried out at 30 kV using i-beam current of 0.26–0.44 nA, depending on area size. Following this, rough milling was performed at acceleration voltage of 30 kV and a current of 20 nA. The resulting cross-sections were polished with a voltage of 30 kV and a current ranging between 1.2 and 2.4 nA. Images were taken using an electron beam at an acceleration voltage of 3 kV and a current of 200 pA, while using immersion mode, thermoluminescent dosimeter detector operated in back-scattered (BS) electron collection mode at a dwell time of 5 µs and 6144 × 4096 pixel² resolution. During sequential sectioning, images were taken every 50 nm using previously mentioned e-beam conditions.

Cell Viability Assay: The viability of cells on substrates was assayed by live–dead staining using a final concentration of 15 µg mL⁻¹ FDA (Sigma-Aldrich) and 5 µg mL⁻¹ PI (Sigma-Aldrich) in media for 5 min at 37 °C. After staining, samples were rinsed with DPBS before being observed under an inverted Ti-S fluorescence microscope (Nikon) using standard filters for FITC (495 nm excitation/517 nm emission) for FDA and tetramethylrhodamine (TRITC, 538 nm excitation/619 nm emission nm) for PI. Five different locations were observed on the surface of each sample at the magnification of 10 × objective lens. All experiments were repeated at least three times.

Flow Cytometry: An LSRIIb flow cytometer (BD) was used to investigate the proliferation, apoptosis, and transfection efficiency of cells harvested from the substrates.

Flow Cytometry—Proliferation Assay: On Day 1, 20 000 cells per well of GPE86, and 40 000 cells per well of L1.2 and Jurkat cells were stained with 5×10^{-6} M CellTrace Violet (CTV) reagent (Invitrogen), seeded onto substrates in 48-well plate and centrifugated at 200 g, 32 °C, 15 min. Substrates carrying cells were then transferred to a new plate with fresh media. After 6 h incubation at 37 °C with 5% CO₂, cells were harvested from the substrates as described above and placed back in fresh media culture. On each of Days 2 and 3, cells were resuspended in FACS buffer (1 × DPBS containing 1% BSA, 2×10^{-3} M EDTA (ethylenediaminetetraacetic acid), and 0.1% sodium azide) and cell proliferation was determined by measuring the fluorescence intensity of CTV using the LSRIIb. Flow cytometry analysis was performed using

405 nm excitation and a 460 nm bandpass emission filter. Unstained cells and CTV-stained cells fixed in FACS buffer after 6 h incubation served as negative and positive controls, respectively.

Flow Cytometry—Apoptosis Assay: An FITC Annexin V/Dead Cell Apoptosis Kit (Thermo Fisher Scientific) with FITC annexin V and PI for flow cytometry for rapid and convenient apoptosis assays was used. 40 000 cells per well of Jurkat cells were seeded onto PDL-coated substrates in 48-well plate, followed by centrifugation at 200 g, 32 °C, 15 min. Substrates carrying cells were transferred to a new plate with fresh media. At 2, 6, 12, and 24 h, cells were harvested from the substrates as described above and stained with the FITC Annexin V/Dead Cell Apoptosis Kit following the manufacture protocol. Stained cells were analyzed on LSRIIb. FITC annexin V and PI were excited using 488 nm laser and detected using 530 and 670 nm filters, respectively.

Loading of Nucleic Acids onto SiNWs: 10 µL of gWiz-GFP or Cy3-gWiz-GFP plasmid DNAs (10, 50, or 100 ng µL^{-1} in H$_2$O; Aldevron) were placed on the PDL-coated substrates and allowed to stand overnight, 4 °C. Cargo-loaded substrates were briefly dried just before cell seeding.

Preparation of Fluorescence Tagged Plasmids: The Label IT Tracker Intracellular Nucleic Acid Localization Kit (Mirus, Japan) was used to add a fluorescence tag to plasmids. 5 µg of gWiz-GFP plasmids were mixed with 2.5 µL of Cy3, 5 µL of labeling buffer A (provided in the Kit), and 37.5 µL of water to make a final volume of 50 µL. The mixture solution was then incubated at 37 °C for 1 h. Cy3-tagged plasmids were then purified using ethanol precipitation.

SiNW-Mediated Cell Transfection: 20 000 cells per well of GPE86, 40 000 cells per well of L1.2 and Jurkat, and 1 00 000 cells per well of primary T cells were seeded onto PDL-coated and cargo-loaded substrates described above in 48-well plate, in 250 µL Opti-MEM (Gibco), followed by centrifugation at 200 g, 32 °C, 15 min. After centrifugation and 6 h incubation at 37 °C in a humidified 5% CO$_2$ atmosphere, substrates carrying cells were gently rinsed, and transferred to new plates. The transfected cells were then detached from the substrates using 0.25% Trypsin/EDTA (Gibco) (adherent cells) or by gently pipetting (suspension cells), and cultured with fresh DMEM or RPMI media (complete DMEM for GPE86 cells, and complete RPMI for L1.2, Jurkat, and primary T cells) for 24–48 h.

Flow Cytometry—Detection of Plasmid Insertion and GFP Expression: Cells were harvested from substrates loaded with plasmids after 6 h incubation. For detection of Cy3 tagged-plasmid insertion, harvested cells were stained with Hoechst (to distinguish from nonliving particles) and PI (to exclude dead cells) and cells were immediately run through flow cytometry analysis. To investigate the transfection efficiency, GFP expression was measured 48 h after harvesting. The excitation/emission wavelengths for Cy3, Hoechst, PI, and GFP on LSRIIb were 561/580, 355/495, 488/670, and 488/540 nm, respectively. Flow cytometry analysis was performed with proper negative and positive controls. Compensation was done to avoid fluorescence leakage between different channels.

Data Processing and Statistical Analysis: Fluorescence microscopy and SEM images were processed and analyzed by NIS-Element (Nikon), Image J, Microscopy Image Browser (MIB, University of Helsinki), and Amira (Thermo Fisher Scientific). Contrast and brightness were not varied from the original pictures. Flow cytometry data were analyzed with FlowJo. All statistical analyses were performed using Prism GraphPad 7. Nonparametric two-sided Mann–Whitney *U*-tests were performed for comparison between two groups. A one-way analysis of variance (ANOVA) was used to calculate univariate data set with more than two groups, and two-way ANOVA tests to calculate multivariate data set. Values are represented as mean and mean ± standard deviation.

Supporting Information

Supporting Information is available from the Wiley Online Library or from the author.

Conflict of Interest

The authors declare no conflict of interest.

[1] a) T. Nagamune, *Nano Convergence* **2017**, *4*, 9; b) S. S. Neelapu, F. L. Locke, N. L. Bartlett, L. J. Lekakis, D. B. Miklos, C. A. Jacobson, I. Braunschweig, O. O. Oluwole, T. Siddiqi, Y. Lin, J. M. Timmerman, P. J. Stiff, J. W. Friedberg, I. W. Flinn, A. Goy, B. T. Hill, M. R. Smith, A. Deol, U. Farooq, P. McSweeney, J. Munoz, I. Avivi, J. E. Castro, J. R. Westin, J. C. Chavez, A. Ghobadi, K. V. Komanduri, R. Levy, E. D. Jacobsen, T. E. Witzig, P. Reagan, A. Bot, J. Rossi, L. Navale, Y. Jiang, J. Aycock, M. Elias, D. Chang, J. Wiezorek, W. Y. Go, *N. Engl. J. Med.* **2017**, *377*, 2531; c) S. Ryu, Y. Matsumoto, T. Matsumoto, T. Ueno, Y. R. Silberberg, C. Nakamura, *Jpn. J. Appl. Phys.* **2018**, *57*, 03EB02.

[2] a) J. Park, B. Andrade, Y. Seo, M.-J. Kim, S. C. Zimmerman, H. Kong, *Chem. Rev.* **2018**, *118*, 1664; b) M. P. Stewart, A. Sharei, X. Ding, G. Sahay, R. Langer, K. F. Jensen, *Nature* **2016**, *538*, 183; c) M. P. Stewart, R. Langer, K. F. Jensen, *Chem. Rev.* **2018**, *118*, 7409.

[3] a) F. Mingozzi, K. A. High, *Nat. Rev. Genet.* **2011**, *12*, 341; b) M. A. Kay, *Nat. Rev. Genet.* **2011**, *12*, 316; c) R. Waehler, S. J. Russell, D. T. Curiel, *Nat. Rev. Genet.* **2007**, *8*, 573.

[4] a) D. Karra, R. Dahm, *J. Neurosci.* **2010**, *30*, 6171; b) J. C. M. van der Loo, J. F. Wright, *Hum. Mol. Genet.* **2016**, *25*, R42.

[5] a) M. A. Mintzer, E. E. Simanek, *Chem. Rev.* **2009**, *109*, 259; b) M. X. Tang, F. C. Szoka, *Gene Ther.* **1997**, *4*, 823; c) V. Vijayanathan, T. Thomas, A. Shirahata, T. J. Thomas, *Biochemistry* **2001**, *40*, 13644.

[6] D. Luo, W. M. Saltzman, *Nat. Biotechnol.* **2000**, *18*, 33.

[7] D. V. Schaffer, N. A. Fidelman, N. Dan, D. A. Lauffenburger, *Biotechnol. Bioeng.* **2000**, *67*, 598.

[8] a) H. Lv, S. Zhang, B. Wang, S. Cui, J. Yan, *J. Controlled Release* **2006**, *114*, 100; b) J. A. Kretzmann, D. C. Luther, M. Norret, V. M. Rotello, K. S. Iyer, in *Targeted Nanosystems for Therapeutic Applications: New Concepts, Dynamic Properties, Efficiency, and Toxicity*, Vol. *1309* (Eds: K. Sakurai, M. A. Ilies), American Chemical Society, Washington, DC **2019**, Ch. 1.

[9] a) R. Capozza, V. Caprettini, C. A. Gonano, A. Bosca, F. Moia, F. Santoro, F. De Angelis, *ACS Appl. Mater. Interfaces* **2018**, *10*, 29107; b) C. Woffendin, Z. Y. Yang, Udaykumar, L. Xu, N. S. Yang,

ADVANCED
SCIENCE NEWS
www.advancedsciencenews.com

NANO · MICRO
small
www.small-journal.com

M. J. Sheehy, G. J. Nabel, *Proc. Natl. Acad. Sci. U. S. A.* **1994**, *91*, 11581.

[10] a) B. Trine, B. Sara, R. R. Katrine, M. Morten Hannibal, B. S. Claus, N. Jesper, L. M. Karen, *Nanotechnology* **2012**, *23*, 415102; b) M. Á. Fernández-Rodríguez, R. Elnathan, R. Ditcovski, F. Grillo, G. M. Conley, F. Timpu, A. Rauh, K. Geisel, T. Ellenbogen, R. Grange, F. Scheffold, M. Karg, W. Richtering, N. H. Voelcker, L. Isa, *Nanoscale* **2018**, *10*, 22189; c) R. Elnathan, L. Isa, D. Brodoceanu, A. Nelson, F. J. Harding, B. Delalat, T. Kraus, N. H. Voelcker, *ACS Appl. Mater. Interfaces* **2015**, *7*, 23717.

[11] Z. C. Lin, C. Xie, Y. Osakada, Y. Cui, B. Cui, *Nat. Commun.* **2014**, *5*, 3206.

[12] a) L. Hanson, W. Zhao, H.-Y. Lou, Z. C. Lin, S. W. Lee, P. Chowdary, Y. Cui, B. Cui, *Nat. Nanotechnol.* **2015**, *10*, 554; b) F. J. Harding, S. Surdo, B. Delalat, C. Cozzi, R. Elnathan, S. Gronthos, N. H. Voelcker, G. Barillaro, *ACS Appl. Mater. Interfaces* **2016**, *8*, 29197.

[13] a) C. Chiappini, E. De Rosa, J. O. Martinez, X. Liu, J. Steele, M. M. Stevens, E. Tasciotti, *Nat. Mater.* **2015**, *14*, 532; b) C. Chiappini, J. O. Martinez, E. De Rosa, C. S. Almeida, E. Tasciotti, M. M. Stevens, *ACS Nano* **2015**, *9*, 5500; c) C. Chiappini, P. Campagnolo, C. S. Almeida, N. Abbassi-Ghadi, L. W. Chow, G. B. Hanna, M. M. Stevens, *Adv. Mater.* **2015**, *27*, 5147; d) A. Banerjee, D. Bernoulli, H. Zhang, M.-F. Yuen, J. Liu, J. Dong, F. Ding, J. Lu, M. Dao, W. Zhang, Y. Lu, S. Suresh, *Science* **2018**, *360*, 300; e) R. Kawamura, M. Miyazaki, K. Shimizu, Y. Matsumoto, Y. R. Silberberg, R. R. Sathuluri, M. Iijima, S. I. Kuroda, F. Iwata, T. Kobayashi, C. Nakamura, *Nano Lett.* **2017**, *17*, 7117; f) Z. Wang, Y. Yang, Z. Xu, Y. Wang, W. Zhang, P. Shi, *Nano Lett.* **2015**, *15*, 7058.

[14] S. Jeong, M. Galic, *Methods Mol. Biol.* **2014**, *1174*, 275.

[15] A. M. Xu, S. A. Kim, D. S. Wang, A. Aalipour, N. A. Melosh, *Lab Chip* **2016**, *16*, 2434.

[16] a) A. V. Melechko, T. E. McKnight, D. K. Hensley, M. A. Guillorn, A. Y. Borisevich, V. I. Merkulov, D. H. Lowndes, M. L. Simpson, *Nanotechnology* **2003**, *14*, 1029; b) T. E. McKnight, A. V. Melechko, D. K. Hensley, D. G. J. Mann, G. D. Griffin, M. L. Simpson, *Nano Lett.* **2004**, *4*, 1213; c) D. G. J. Mann, T. E. McKnight, J. T. McPherson, P. R. Hoyt, A. V. Melechko, M. L. Simpson, G. S. Sayler, *ACS Nano* **2008**, *2*, 69; d) W. Kim, J. K. Ng, M. E. Kunitake, B. R. Conklin, P. Yang, *J. Am. Chem. Soc.* **2007**, *129*, 7228.

[17] a) A. K. Shalek, J. T. Robinson, E. S. Karp, J. S. Lee, D.-R. Ahn, M.-H. Yoon, A. Sutton, M. Jorgolli, R. S. Gertner, T. S. Gujral, G. MacBeath, E. G. Yang, H. Park, *Proc. Natl. Acad. Sci. U. S. A.* **2010**, *107*, 1870; b) A. K. Shalek, J. T. Gaublomme, L. Wang, N. Yosef, N. Chevrier, M. S. Andersen, J. T. Robinson, N. Pochet, D. Neuberg, R. S. Gertner, I. Amit, J. R. Brown, N. Hacohen, A. Regev, C. J. Wu, H. Park, *Nano Lett.* **2012**, *12*, 6498; c) M. Choi, S. H. Lee, W. B. Kim, V. Gujrati, D. Kim, J. Lee, J.-I. Kim, H. Kim, P. E. Saw, S. Jon, *Adv. Healthcare Mater.* **2016**, *5*, 101; d) B. G. Nair, K. Hagiwara, M. Ueda, H.-H. Yu, H.-R. Tseng, Y. Ito, *ACS Appl. Mater. Interfaces* **2016**, *8*, 18693.

[18] a) R. Kawamura, K. Shimizu, Y. Matsumoto, A. Yamagishi, Y. R. Silberberg, M. Iijima, S. Kuroda, K. Fukazawa, K. Ishihara, C. Nakamura, *J. Nanobiotechnol.* **2016**, *14*, 74; b) D. Matsumoto, R. R. Sathuluri, Y. Kato, Y. R. Silberberg, R. Kawamura, F. Iwata, T. Kobayashi, C. Nakamura, *Sci. Rep.* **2015**, *5*, 15325; c) S. Choi, H. Kim, S. Y. Kim, E. G. Yang, *Nanoscale* **2016**, *8*, 11380.

[19] K. H. Kim, J. Kim, J. S. Choi, S. Bae, D. Kwon, I. Park, D. H. Kim, T. S. Seo, *Small* **2015**, *11*, 6215.

[20] M. S. Chan, P. K. Lo, *Small* **2014**, *10*, 1255.

[21] S. Park, Y.-S. Kim, W. B. Kim, S. Jon, *Nano Lett.* **2009**, *9*, 1325.

[22] N. Yosef, A. K. Shalek, J. T. Gaublomme, H. Jin, Y. Lee, A. Awasthi, C. Wu, K. Karwacz, S. Xiao, M. Jorgolli, D. Gennert, R. Satija,

A. Shakya, D. Y. Lu, J. J. Trombetta, M. R. Pillai, P. J. Ratcliffe, M. L. Coleman, M. Bix, D. Tantin, H. Park, V. K. Kuchroo, A. Regev, *Nature* **2013**, *496*, 461.

[23] a) W. Zhao, L. Hanson, H.-Y. Lou, M. Akamatsu, P. D. Chowdary, F. Santoro, J. R. Marks, A. Grassart, D. G. Drubin, Y. Cui, B. Cui, *Nat. Nanotechnol.* **2017**, *12*, 750; b) R. Elnathan, M. Kwiat, F. Patolsky, N. H. Voelcker, *Nano Today* **2014**, *9*, 172.

[24] a) X. Xie, A. M. Xu, M. R. Angle, N. Tayebi, P. Verma, N. A. Melosh, *Nano Lett.* **2013**, *13*, 6002; b) I. Obataya, C. Nakamura, Han, N. Nakamura, J. Miyake, *Nano Lett.* **2005**, *5*, 27.

[25] Y. Wang, Y. Yang, L. Yan, S. Y. Kwok, W. Li, Z. Wang, X. Zhu, G. Zhu, W. Zhang, X. Chen, P. Shi, *Nat. Commun.* **2014**, *5*, 4466.

[26] S. Qi, C. Yi, S. Ji, C.-C. Fong, M. Yang, *ACS Appl. Mater. Interfaces* **2009**, *1*, 30.

[27] a) H. Persson, Z. Li, J. O. Tegenfeldt, S. Oredsson, C. N. Prinz, *Sci. Rep.* **2015**, *5*, 18535; b) N. Buch-Månson, S. Bonde, J. Bolinsson, T. Berthing, J. Nygård, K. L. Martinez, *Adv. Funct. Mater.* **2015**, *25*, 3246; c) N. Buch-Manson, D. H. Kang, D. Kim, K. E. Lee, M. H. Yoon, K. L. Martinez, *Nanoscale* **2017**, *9*, 5517.

[28] Y. Coffinier, R. Boukherroub, in *Semiconducting Silicon Nanowires for Biomedical Applications* (Ed: J. L. Coffer), Woodhead Publishing, Sawston, Cambridge **2014**, p. 26.

[29] X. Xie, A. Aalipour, S. V. Gupta, N. A. Melosh, *ACS Nano* **2015**, *9*, 11667.

[30] a) A. M. Xu, A. Aalipour, S. Leal-Ortiz, A. H. Mekhdjian, X. Xie, A. R. Dunn, C. C. Garner, N. A. Melosh, *Nat. Commun.* **2014**, *5*, 3613; b) F. Santoro, W. Zhao, L.-M. Joubert, L. Duan, J. Schnitker, Y. van de Burgt, H.-Y. Lou, B. Liu, A. Salleo, L. Cui, Y. Cui, B. Cui, *ACS Nano* **2017**, *11*, 8320; c) M. Dipalo, A. F. McGuire, H.-Y. Lou, V. Caprettini, G. Melle, G. Bruno, C. Lubrano, L. Matino, X. Li, F. De Angelis, B. Cui, F. Santoro, *Nano Lett.* **2018**, *18*, 6100.

[31] S. Gopal, C. Chiappini, J. Penders, V. Leonardo, H. Seong, S. Rothery, Y. Korchev, A. Shevchuk, M. M. Stevens, *Adv. Mater.* **2019**, *31*, 1806788.

[32] a) C. N. Prinz, *J. Phys.: Condens. Matter* **2015**, *27*, 233103; b) X. Shi, A. von dem Bussche, R. H. Hurt, A. B. Kane, H. Gao, *Nat. Nanotechnol.* **2011**, *6*, 714.

[33] C. S. Hansel, S. W. Crowder, S. Cooper, S. Gopal, M. João Pardelha da Cruz, L. de Oliveira Martins, D. Keller, S. Rothery, M. Becce, A. E. G. Cass, C. Bakal, C. Chiappini, M. M. Stevens, *ACS Nano* **2019**, *13*, 2913.

[34] J. T. Parsons, A. R. Horwitz, M. A. Schwartz, *Nat. Rev. Mol. Cell Biol.* **2010**, *11*, 633.

[35] a) K. L. Mui, C. S. Chen, R. K. Assoian, *J. Cell Sci.* **2016**, *129*, 1093; b) S. K. Sastry, K. Burridge, *Exp. Cell Res.* **2000**, *261*, 25.

[36] J. L. Bays, K. A. DeMali, *Cell. Mol. Life Sci.* **2017**, *74*, 2999.

[37] a) S. Pogodin, V. A. Baulin, *ACS Nano* **2010**, *4*, 5293; b) H. Kagiwada, C. Nakamura, T. Kihara, H. Kamiishi, K. Kawano, N. Nakamura, J. Miyake, *Cytoskeleton* **2010**, *67*, 496; c) D. Lechardeur, A. S. Verkman, G. L. Lukacs, *Adv. Drug Delivery Rev.* **2005**, *57*, 755.

[38] L. He, E. J. Sayers, P. Watson, A. T. Jones, *Sci. Rep.* **2018**, *8*, 7318.

[39] a) P. M. Wu, N. Anttu, H. Q. Xu, L. Samuelson, M.-E. Pistol, *Nano Lett.* **2012**, *12*, 1990; b) T. Berthing, S. Bonde, K. R. Rostgaard, M. H. Madsen, C. B. Sørensen, J. Nygård, K. L. Martinez, *Nanotechnology* **2012**, *23*, 415102.

[40] A. Aalipour, A. M. Xu, S. Leal-Ortiz, C. C. Garner, N. A. Melosh, *Langmuir* **2014**, *30*, 12362.

[41] R. G. Parton, M. A. del Pozo, *Nat. Rev. Mol. Cell Biol.* **2013**, *14*, 98.

[42] B. Sinha, D. Köster, R. Ruez, P. Gonnord, M. Bastiani, D. Abankwa, R. V. Stan, G. Butler-Browne, B. Vedie, L. Johannes, N. Morone, R. G. Parton, G. Raposo, P. Sens, C. Lamaze, P. Nassoy, *Cell* **2011**, *144*, 402.

[43] G. Golani, N. Ariotti, R. G. Parton, M. M. Kozlov, *Dev. Cell* **2019**, *48*, 523.

ADVANCED
SCIENCE NEWS

www.advancedsciencenews.com

NANO · MICRO

small

www.small-journal.com

[44] R. Elnathan, B. Delalat, D. Brodoceanu, H. Alhmoud, F. J. Harding, K. Buehler, A. Nelson, L. Isa, T. Kraus, N. H. Voelcker, *Adv. Funct. Mater.* **2015**, *25*, 7215.

[45] M. van Engeland, L. J. W. Nieland, F. C. S. Ramaekers, B. Schutte, C. P. M. Reutelingsperger, *Cytometry* **1998**, *31*, 1.

[46] A. Bouter, C. Gounou, R. Bérat, S. Tan, B. Gallois, T. Granier, B. L. d'Estaintot, E. Pöschl, B. Brachvogel, A. R. Brisson, *Nat. Commun.* **2011**, *2*, 270.

[47] J. D. Tario Jr., A. N. Conway, K. A. Muirhead, P. K. Wallace, *Methods Mol. Biol.* **2018**, *1678*, 249.

[48] J. C. Tempany, J. H. S. Zhou, P. D. Hodgkin, V. L. Bryant, *Immunol. Cell Biol.* **2018**, *96*, 149.

[49] R. Rattan, A. U. Bielinska, M. M. Banaszak Holl, *J. Gene Med.* **2014**, *16*, 75.

[50] a) S. Hama, H. Akita, R. Ito, H. Mizuguchi, T. Hayakawa, H. Harashima, *Mol. Ther.* **2006**, *13*, 786; b) J. Zabner, A. J. Fasbender, T. Moninger, K. A. Poellinger, M. J. Welsh, *J. Biol. Chem.* **1995**, *270*, 18997.

[51] R. F. Shearer, D. N. Saunders, *Genes Cells* **2015**, *20*, 1.

[52] D. Sauce, M. Bodinier, M. Garin, B. Petracca, N. Tonnelier, A. Duperrier, J. V. Melo, J. F. Apperley, C. Ferrand, P. Hervé, F. Lang, P. Tiberghien, E. Robinet, *Blood* **2002**, *99*, 1165.

[53] S. Cavalieri, S. Cazzaniga, M. Geuna, Z. Magnani, C. Bordignon, L. Naldini, C. Bonini, *Blood* **2003**, *102*, 497.

[54] C. Ferrand, E. Robinet, E. Contassot, J.-M. Certoux, A. Lim, P. Hervé, P. Tiberghien, *Hum. Gene Ther.* **2000**, *11*, 1151.

[55] a) W. R. Drobyski, D. Majewski, K. Ozker, G. Hanson, *J. Immunol.* **1998**, *161*, 2610; b) E. Contassot, W. Murphy, R. Angonin, J.-J. Pavy, M. C. Bittencourt, É. Robinet, C. W. Reynolds, J.-Y. Cahn, P. Hervé, P. Tiberghien, *Transplantation* **1998**, *65*, 1365.